Title

Distinct solubility and cytotoxicity regimes of paclitaxel-loaded cationic liposomes at low and high drug content revealed by kinetic phase behavior and cancer cell viability studies.

Authors

Steffes, Victoria

Murali, Meena

Park, Yoonsang

et al.

Publication Date

2017-11-01

DOI

10.1016/j.biomaterials.2017.08.026

Peer reviewed

HHS Public Access

Author manuscript

Biomaterials. Author manuscript; available in PMC 2018 November 01.

Published in final edited form as:

Biomaterials. 2017 November ; 145: 242–255. doi:10.1016/j.biomaterials.2017.08.026.

Distinct Solubility and Cytotoxicity Regimes of Paclitaxel-Loaded Cationic Liposomes at Low and High Drug Content Revealed by Kinetic Phase Behavior and Cancer Cell Viability Studies

Victoria M. Steffes[a,b], **Meena M. Murali**[b], **Yoonsang Park**[b,c], **Bretton J. Fletcher**[b], **Kai K. Ewert**[b], and **Cyrus R. Safinya**[*,b]

[a]Chemistry and Biochemistry Department, University of California, Santa Barbara, CA 93106, USA

[b]Materials, Physics, and Molecular, Cellular & Developmental Biology Department, University of California, Santa Barbara, CA 93106, USA

Abstract

Lipid-based particles are used worldwide in clinical trials as carriers of hydrophobic paclitaxel (PTXL) for cancer chemotherapy, albeit with little improvement over the standard-of-care. Improving efficacy requires an understanding of intramembrane interactions between PTXL and lipids to enhance PTXL solubilization and suppress PTXL phase separation into crystals. We studied the solubility of PTXL in cationic liposomes (CLs) composed of positively charged 2,3-dioleyloxypropyltrimethylammonium chloride (DOTAP) and neutral 1,2-dioleoyl-*sn*-glycero-3-phosphatidylcholine (DOPC) as a function of PTXL membrane content and its relation to efficacy. Time-dependent kinetic phase diagrams were generated from observations of PTXL crystal formation by differential-interference-contrast microscopy. Furthermore, a new synchrotron small-angle x-ray scattering *in situ* methodology applied to DOTAP/DOPC/PTXL membranes condensed with DNA enabled us to detect the incorporation and time-dependent depletion of PTXL from membranes by measurements of variations in the membrane interlayer and DNA interaxial spacings. Our results revealed three regimes with distinct time scales for PTXL membrane solubility: hours for > 3 mol% PTXL (low), days for ≈ 3 mol% PTXL (moderate), and ≥ 20 days for < 3 mol% PTXL (long-term). Cell viability experiments on human cancer cell lines using CL_{PTXL} nanoparticles (NPs) in the distinct CL_{PTXL} solubility regimes reveal an unexpected dependence of efficacy on PTXL content in NPs. Remarkably, formulations with lower PTXL content and thus higher stability show higher efficacy than those formulated at the membrane

[*]Corresponding Author: Safinya@mrl.ucsb.edu.

[c]Present address: Department of Materials Science and Engineering, Pennsylvania State University, University Park, PA 16802, USA

Supplementary Data. Experimental data for an IC-50 determination for each cell line (M21 and PC3), a comparison of the efficacy of free and liposomal PTXL, efficacy data as a function of PTXL content to supplement the data in Fig. 7, as well as a table with all peak positions for the x-ray scattering data shown in Figures 4b and 5.

solubility limit of ≈ 3 mol% PTXL (which has been the focus of most previous physicochemical studies and clinical trials of PTXL-loaded CLs). Furthermore, an additional high-efficacy regime is seen on occasion for liposome compositions with PTXL ≥ 9 mol% applied to cells at short time scales (hours) after formation. At longer time scales (days), CL_{PTXL} NPs with ≥ 3 mol% PTXL lose efficacy while formulations with 1–2 mol% PTXL maintain high efficacy. Our findings underscore the importance of understanding the relationship of the kinetic phase behavior and physicochemical properties of CL_{PTXL} NPs to efficacy.

Keywords

Liposome; nanoparticle; paclitaxel; hydrophobic drug; drug delivery; cancer chemotherapy

Introduction

The landmark discovery that paclitaxel (PTXL), derived from the Pacific Yew tree, suppresses cell division in tumors [1], has resulted in the ongoing worldwide effort to develop efficient synthetic carriers of PTXL for cancer chemotherapy [2]. PTXL is a hydrophobic molecule (Figure 1a, b) known to inhibit mitosis by stabilizing microtubules (upon binding a specific hydrophobic pocket on the β-tubulin subunit), thereby obstructing chromosome capture and segregation during mitosis and subsequently activating apoptotic signaling pathways that lead to cell death [3–8]. PTXL is among the most common drugs used to treat ovarian, breast, lung, pancreatic, and other cancers and is included in the World Health Organization's List of Essential Medicines [9–13]. PTXL is commonly administered in the form of Taxol®, where it is solubilized for delivery in Kollifor-EL (formerly Cremophor EL), which causes hypersensitivity reactions and delivers PTXL non-discriminately throughout the body [14–16]. In 2005, nanoparticle albumin-bound PTXL was approved by the FDA (Abraxane®); this formulation is considered to have fewer adverse reactions than Taxol, although there are mixed reports on whether it improves survival outcomes [17–19].

Considering its biochemical mechanism of action, PTXL should be effective against most cancer cells. Therefore, its lack of efficacy against some cancers is likely caused by the inadequacies of the available drug delivery vehicles. There are various examples in the literature that demonstrate that the drug carrier is a contributing factor in determining which cancers a treatment will be effective against. For example, PEGylated liposomal doxorubicin (DOX) has proven to be more effective than conventional DOX administration to treat AIDS-related Kaposi's sarcoma [20]. PTXL in the form of Abraxane appears to be effective to treat metastatic melanoma, whereas the Taxol formulation is not [21]. Thus, development of novel drug delivery agents for established drugs may open new treatment avenues against an expanded range of cancers.

Liposomal nanoparticles (NPs) are versatile drug delivery agents due to their ability to sequester multiple distinct therapeutic molecules, including long and short nucleic acids (electrostatically condensed with membranes) [22], as well as hydrophilic and hydrophobic drugs in different forms (solubilized, crystallized, surface-conjugated) [23]. Because each

therapeutic drug molecule possesses unique physical and chemical characteristics, its liposomal carrier must be tailored to these properties to achieve efficient delivery [24].

Studies suggest that longer retention times of an anticancer drug within circulating liposomes leads to greater accumulation of the drug at tumor sites [25,26]. Much of this work has been done using DOX and other drugs that can be loaded efficiently in the interior aqueous pocket of liposomes (e.g. Doxil and Myocet) [27]. To prolong retention of these drugs in liposomes, the current approach is to increase the rigidity of the membrane and thereby reduce its permeability to hydrophilic drugs, by employing lipids with high melting points (e.g. with saturated tails) and including cholesterol.

Hydrophobic drugs, on the other hand, are solubilized by and reside directly in the nonpolar (hydrocarbon chain) region of the membrane (Fig. 1b, c). These drugs, which include PTXL, are quickly expelled from membranes consisting of saturated lipid tails or those that have a high concentration of cholesterol [28–33]. This observation indicates that the maximum loading and residence time of hydrophobic drugs within liposomes are particularly sensitive to the liposome composition. A key concern is that hydrophobic drugs will leach out of liposomes quickly *in vivo* because they reside at the particle boundary rather than the interior, and will subsequently bind to plasma proteins with hydrophobic pockets acting as ‘lipid sinks’ [23,26,34].

Various studies indicate that liposome–PTXL formulations exhibit lower toxicity compared to Taxol®, may increase the maximum tolerated drug dose, and may improve biodistribution [30,35–38]. One liposomal formulation of PTXL is approved in China (Lipusu®) [39,40], while others are in clinical trials. Composition information for the Lipusu formulation is not publically available. LEP-ETU is in Phase II trials in the United States; it is an anionic lipid-based carrier composed of the neutral lipid DOPC (1,2-dioleoyl-*sn*-glycero-3-phosphatidylcholine), cholesterol, and cardiolipin (90:5:5 mole ratio) with an additional 3 mol% PTXL [41]. EndoTAG-1 is in Phase III trials in Taiwan and has a cationic liposome structure consisting of the univalent cationic lipid 2,3-dioleyloxypropyltrimethylammonium chloride (DOTAP), DOPC, and PTXL (50:47:3 mole ratio) [28]. Other types of PTXL-containing liposomes (e.g. PEGylated, antibody-targeted) have shown some promising early results, but have not progressed to clinical trials [30,35,42–45].

Straubinger has reported that 3 mol% is the solubility limit for PTXL in liposomes, above which PTXL rapidly precipitates [46]. However, there are few studies that systematically evaluate this drug loading parameter as a function of lipid and membrane properties and none that demonstrate that liposomes at this limit are the most efficient at actual drug delivery. Studies from various groups have investigated the behavior of PTXL in different types of membranes—cationic, anionic, neutral, cholesterol-containing, saturated, and PEGylated—but these studies are few in number and together form a very fragmented and sometimes contradictory picture [29–32,44,47]. What is lacking is a comprehensive study of how the physicochemical properties of liposome–PTXL particles, including their time-dependent phase behavior, correlate to PTXL membrane content for optimal drug delivery and efficacy (i.e. ability to induce cancer cell death).

Cationic liposomes (CLs) are of particular interest because the electrostatic attraction between positive particles and the negatively charged sulfated proteoglycans (components of the glycocalyx which covers cells) leads to cell binding. Studies suggest that positively charged particles may achieve some cancer-specific targeting because the tumor neovasculature is more negatively charged than other tissues in the body and will therefore accumulate cationic particles at a higher concentration [42,48–50]. This assertion was the basis for choosing the lipid mixture of EndoTAG-1 as a starting point in our investigation of PTXL–lipid interactions.

In the work reported here, we generated kinetic phase diagrams characterizing the time-dependent phase separation and crystal formation of PTXL as a function of PTXL content in DOTAP/DOPC membranes. The phase diagrams were generated from direct observations of PTXL crystallization using differential-interference-contrast (DIC) microscopy. To corroborate this data, we used high-resolution synchrotron small-angle x-ray scattering (SAXS), which unambiguously identified the PTXL crystals by their characteristic diffraction peaks. Furthermore, SAXS allowed us to perform *in situ* measurements of variations in the membrane interlayer and DNA interaxial spacings in multilamellar, onion-like complexes of cationic DOTAP/DOPC/PTXL membranes condensed with DNA, confirming both incorporation of PTXL and its depletion from the membranes upon crystallization.

The kinetic phase diagrams show a solubility threshold at 3 mol% PTXL content: below 3 mol%, PTXL exhibits long-term solubility (≥ 20 days) in unsonicated CLs, whereas above 3 mol%, the drug crystallizes within the first day following hydration. PTXL remained soluble in CLs on a time scale of days when incorporated at 3 mol%. The duration of PTXL solubility in CL_{PTXL} NPs consisting of small (< 200 nm diameter) unilamellar liposomes (produced by sonication) is shorter than in unsonicated (uni- and multi-lamellar) liposomes with a broad distribution of larger sizes (average diameter ≈ 800 nm) over the whole range of PTXL contents tested.

While previous studies seem to empirically choose one or two PTXL–liposome formulations based on physical characterization alone to push forward directly into animal testing, our study breaks from that approach and instead attempts to correlate the extent of biological response to the liposome properties. Thus, we assessed efficacy *in vitro* for a series of CL_{PTXL} NPs with varying PTXL content in the CL membranes (at fixed total PTXL concentration in solution) by measuring human cancer cell survival. We observed new drug delivery behavior dependent both on the PTXL content (i.e., PTXL loading) and the timing of drug delivery after liposome hydration (at short (hours) vs. long (days) times). CL_{PTXL} NPs that exhibit long-term solubility (PTXL content ≤ 2 mol%) show the highest efficacy (extent of cell death), whether delivered hours or days after liposome hydration. In the majority of experiments, CL_{PTXL} NPs containing ≥ 9 mol% PTXL exhibited greater efficacy than NPs with 3–7 mol% PTXL when the particles were applied to cells within a few hours of hydration. This effect disappears over time, as PTXL phase-separates and crystalizes. Thus, whereas previous studies (including clinical trials) of CL-based carriers have exclusively focused on 3 mol% PTXL content (i.e. near the CL solubility limit) [35,41,51], our study has revealed two distinctly new PTXL composition regimes, below and above 3

mol% PTXL content, where CL_{PTXL} NPs exhibit improved efficacy. Furthermore, our results demonstrate that the time of NP delivery after liposome hydration is a critical parameter affecting efficacy.

Materials and Methods

Materials

Lipid stock solutions of DOPC and DOTAP in chloroform were purchased from Avanti Polar Lipids. PTXL was purchased from Acros Organics and dissolved in chloroform at 10.0 mM concentration. CellTiter 96® AQueous-One Solution Cell Proliferation Assay was obtained from Promega. Paclitaxel–Oregon Green® 488 Conjugate, Texas Red–DHPE, and glycerol monooleate (GMO) were purchased from Thermo Fisher Scientific as powders and dissolved in chloroform to 190 μM, 81 μM and 10 mM concentrations, respectively. Custom DNA oligomers (sense strand: ACGCTTT; antisense strand: AGCGTTT) were purchased from Sigma-Aldrich. Luciferase plasmid pGL3 (purchased from Promega) was propagated in *Escherichia coli* and purified using a Qiagen Plasmid Mega Prep Kit.

Cell Culture

The human cell lines PC3 (ATCC number: CRL-1435; prostate cancer) and M21 (melanoma) were gifts from the Ruoslahti Lab (Burnham Institute, La Jolla). M21 cells are a subclone that was derived in the laboratory of Dr. Ralph Reisfeld (Scripps Institute, La Jolla) from the human melanoma line UCLA-SO-M21, which was originally provided by Dr. D. L. Morton (UCLA, Los Angeles). Cells were cultured in DMEM (Invitrogen) supplemented with 10% fetal bovine serum (Gibco) and 1% penicillin/streptomycin (Invitrogen). Cells were passaged every 72 h to maintain subconfluency and kept in an incubator at 37 °C in a humidified atmosphere containing 5% CO_2.

Liposome preparation

Mixed solutions of lipid and PTXL were prepared in chloroform:methanol (3:1, v/v) in small glass vials at a total molar concentration (lipid + PTXL) of 1 mM for cell experiments, 5 mM for DIC microscopy, and 20 mM for x-ray experiments. Individual stock solutions were combined according to the desired molar composition; typically, the cationic lipid DOTAP content remained constant for comparison, while neutral DOPC was exchanged for PTXL as the amount of PTXL was varied. The organic solvent was evaporated by a stream of nitrogen for 10 min and dried further in a vacuum (rotary vane pump) for 16 h. The resulting lipid/PTXL films were hydrated with high-resistivity water (18.2 MΩcm) to the aforementioned concentrations. Immediately thereafter, suspensions were agitated with a tip sonicator (Sonics and Materials Inc. Vibra Cell, set to 30 Watt output) for 7 min to form small unilamellar vesicles (“sonicated liposomes”).

Dynamic Light Scattering

A Malvern Zetasizer Nano ZS was used to measure the average size of the liposomes. A total of 100 μL of a 5 mM stock suspension was diluted with 900 μL of DMEM to mimic the salt conditions of the liposomes in solution when they are added to cells. This solution was

loaded into a DLS cuvette (Malvern DTS1070) and measured. The liposome diameter is reported as the average ± standard deviation of 3 measurements.

Polarized optical microscopy

Liposome samples at a concentration of 5 mM were loaded into flat microslides (VitroCom) via capillary action and sealed on both ends with 5-min epoxy glue. Samples were observed under crossed polarizers on a Nikon Optiphot microscope with a 5× objective.

DIC microscopy

Samples prepared at 5 mM concentration were mixed manually after hydration by agitating the vial to ensure homogenous mixing. The sample solutions were stored at 37 °C for the duration of the experiment. At predetermined times, 2 μL aliquots were withdrawn, placed on microscope slides, covered by a coverslip kept in place by vacuum grease, and imaged at 10 or 20× magnification on an inverted Diaphot 300 (Nikon) microscope. The samples were first imaged within minutes of adding water to the dried lipid films, then every 2 h until 12 h, every 12 h until 72 h, and daily thereafter until PTXL crystals were observed or the entire sample was used up. The kinetic phase diagrams report an average time of PTXL solubility based on 2–4 independently formed samples for each mol% PTXL.

Fluorescence microscopy

Liposomes were prepared as described above at 5 mM total concentration, except for the incorporation of two fluorophores, one for lipid and one for PTXL. The liposome composition was DOTAP:DOPC:OregonGreen–PTXL:TexasRed–DHPE=90:10:5:7.1 (molar ratio). An aliquot of 2 μL of this solution was placed between glass coverslip and slide and sealed in with vacuum grease. The solution was imaged with a Nikon Diaphot 300 equipped with a Nikon 1.4 NA 60× Plan Apo DIC Objective and a PCO Sensicam QE CCD camera.

X-ray scattering

X-ray scattering experiments were performed at the Stanford Synchrotron Radiation Lightsource (Beamline 4-2) with an x-ray energy of 9 keV and a sample–detector distance of 1.2 m. Lipid/PTXL films were prepared as described for liposome preparation (30 mol% DOTAP, 70–x_{PTXL} mol% DOPC). After hydration (to 20 mM, i.e., 6 mM DOTAP), lipid suspensions were placed in a bath sonicator for 30 min and then stored at room temperature. To prepare samples for x-ray scattering, aliquots of the liposome suspensions were mixed in 1.5 mm quartz capillaries (Hilgenberg) with calf thymus DNA solution (5 mg/mL in water) at a lipid/DNA charge ratio of 1.5. Samples were centrifuged in a capillary rotor in a Universal 320R centrifuge (Hettich, Germany) at 14,000 *g* for 30 min and the condensed lipid–DNA phase pelleted to the bottom of the x-ray capillary along with any PTXL crystals already present. Condensation of liposomes into CL–DNA complexes is expected to introduce confinement of crystal growth, which would complicate crystal detection by scattering. Thus, CL–DNA complexes were prepared immediately prior to measurement for each time point for each liposome composition under investigation, with the expectation that

complex formation and centrifugation would break up newly formed crystals and disperse them heterogeneously into the CL–DNA pellet.

Concentrated lipid solutions with high PTXL content *without DNA* also produced opaque white pellets when centrifuged. X-ray scattering confirmed that these contained phase-separated PTXL. These results, shown in Figure 4a, are for samples using GMO as the neutral lipid in place of DOPC. The lipid only sample was DOTAP:GMO (50:50 mole ratio), while the PTXL sample had the composition DOTAP:GMO:PTXL (50:44:6 mole ratio).

Cell viability assays

Cells were plated in 96-well plates at a density of 5,000 cells/well. Cells were incubated overnight to adhere to the plate. Liposome suspensions were diluted in DMEM to reach the desired concentration of PTXL. The cell culture medium was then manually removed from the wells with a pipette (rather than a vacuum aspirator; to ensure that cells were not removed unintentionally) and replaced with 100 μL of the liposome suspension. After incubation for 24 h, the liposome-containing medium was removed manually with a pipette and replaced with supplemented DMEM. After incubation for another 48 h, the cell viability was measured with the CellTiter 96® AQueous-One Solution Cell Proliferation Assay (Promega). The assay solution was diluted 6-fold with DMEM and 120 μL of this solution were added to each well. The absorbance at 490 nm was measured with a plate reader (Tecan M220) after 1 h of incubation as per the assay instructions. Each data point is the average of four identically treated wells and reported as a percentage of the viability of untreated cells. The incubation times in this procedure are based on previous experiments by L. Wilson (UCSB) that were reproduced in our lab and showed that the viability of cells treated with PTXL relative to control cells decreases over time until reaching a plateau at around 72 h [4].

For cell viability experiments comparing the efficacy of CL_{PTXL} NPs to CL_{PTXL}-DNA complexes, two batches of liposomes were prepared with either 30 or 50 mol% DOTAP, 3 mol% PTXL, and the remainder DOPC. Complexes were formed by mixing the cationic lipid with negatively charged DNA at a positive charge ratio of 5. Two types of DNA were used: a large luciferase plasmid DNA and a short double-stranded DNA 5 base pairs long, with 2 extra unpaired thymine residues at the 3′ end of each strand to minimize end-to-end DNA sticking [52]. Liposomes and DNA were each diluted in DMEM before subsequent mixing. Particles were added to cells such that the amount of PTXL delivered to each cell culture well was constant.

In viability experiments comparing CL_{PTXL} NPs of varying PTXL content, the total concentration of PTXL was kept constant (at the approximate IC-50, see text). This results in varying lipid concentrations. For example, delivering a fixed PTXL concentration of 40 nM in a volume of 100 μL at 1 and 9 mol% PTXL results in a total lipid concentration of 4 and 0.44 μM, respectively.

To assess the effect of time after hydration on the efficacy of CL_{PTXL} NPs, seven vials with CL/PTXL films were prepared as described above for each of the formulations (50 mol% DOTAP, 50–x_{PTXL} mol% DOPC) under investigation. These films were hydrated and

sonicated over the course of 10 d (0, 1, 2, 4, 6, 8, and 10 d before addition to cells). On the day the CL_{PTXL} NPs were added to cells, each suspension was first diluted in DMEM to a final PTXL concentration of 22.5 nM for PC-3 cells and 65.0 nM for M21 cells. The solutions were then used in the cell viability assay as described above.

Results and Discussion

Microscopy Characterization of PTXL-Loaded Cationic Liposomes

As described in the Introduction, hydrophobic drugs are expected to partition into the membrane of liposomes. Our x-ray scattering data (see below, discussion of Fig. 6) confirms this for PTXL in CLs. To visualize the partitioning, we carried out fluorescence colocalization experiments. Figure 1(d–g) shows representative images of the results: part (d) displays a DIC optical image of a giant cationic liposome (composed of DOTAP:DOPC:OregonGreen–PTXL:TexasRed–DHPE at a 90:10:5:7.1 mole ratio); part (e) shows the green fluorescence from the Oregon Green® 488–PTXL conjugate; part (f) shows the red fluorescence due to lipid label TexasRed–DHPE; part (g) shows the overlay of the fluorescence of lipid label and PTXL-conjugate. This series of images demonstrates that fluorescent PTXL and lipid are colocalized and concentrated along the outer edge of the liposome, consistent with the PTXL conjugate residing within the hydrophobic region of the bilayer. The fluorescent PTXL conjugate thus behaves similarly in this respect to PTXL. However, the Oregon Green® 488–PTXL conjugate is not a suitable PTXL analog for the quantitative study of the stability of PTXL in CL formulations because its chemical properties are significantly altered by the addition of the fluorophore. For example, while the conjugate can be used to image microtubules, it is applied to cells at a much higher concentration than lethal doses of unaltered PTXL, suggesting it is much less toxic. In addition, the fluorophore-conjugated PTXL is more water soluble than PTXL and does not readily phase-separate from the CL membranes to form crystals. This shows that caution is required in the use of fluorescently-tagged hydrophobic drugs for quantitative studies. We therefore used the unaltered form of PTXL (Figure 1a, b) for the remainder of our studies.

Various groups have reported 3 mol% PTXL as the solubility limit in liposomes [41,46]. Beyond this limit, PTXL phase-separates and forms characteristic needle-shaped crystals. Figure 1h shows a low-magnification polarized optical micrograph displaying such crystals in an unsonicated CL_{PTXL} sample 5 days after hydration. While previous studies have largely relied on multi-step HPLC experiments to monitor drug loading and retention over time [30,31,43], we set out to establish a DIC microscopy-based experimental protocol that would allow us to determine the PTXL stability in novel lipid formulations with higher throughput.

Nucleation and crystal growth theory, along with our experimental observations, suggests that the rate-limiting step in PTXL crystallization is nucleation, with crystal growth occurring on a much faster time scale thereafter. The experimental evidence supporting this is that the size of the crystals we observe in DIC microscopy is about 20 μm or larger. The resolution limit of DIC microscopy is much smaller, but we do not see evidence of smaller PTXL crystals. This suggests that the crystals grow to their large size very rapidly or, in other words, that nucleation is the rate-limiting step. Thus, direct observation of PTXL

crystals using DIC microscopy is an appropriate technique to assess CL_{PTXL} stability on the relevant time scale of hours to days. Figure 2 provides examples of DIC micrographs of CL_{PTXL} liposomes before and after PTXL crystallization. The pictured samples consisted of 30 mol% DOTAP, 1.25–5 mol% PTXL, and the remainder DOPC. Two methods of sample preparation were used: unsonicated liposomes as formed spontaneously upon hydration, which are larger and display a broad size distribution, and sonicated liposomes, which display a more monodisperse distribution of smaller sizes.

Figure 2(a–c) displays images obtained for a sample in which the PTXL crystallizes in a matter of hours. The image shown in part (a) was taken 2 h after liposome hydration and shows no evidence of phase separation and crystal formation, while the images in parts (b) and (c) show PTXL crystals and an axialite bundle of crystals at 4 and 6 h, respectively. At lower PTXL content (4 mol%), CL_{PTXL} NPs are stable for longer periods, with PTXL crystals appearing between 12 h and 24 h (Figure 2d). The images in Figure 2e (2 mol% PTXL) and 2f (1.5 mol% PTXL) contrast the two sample preparation methods (sonicated (2e) and unsonicated (2f)) for two formulations at even lower PTXL content. These CL_{PTXL} NPs exhibited long term stability, with no crystals detectable by DIC microscopy even 16 days (Figure 2e) and 21 days (Figure 2f) after hydration. As is evident in the DIC images, unsonicated samples contain a broad distribution of particle sizes, up to tens of micrometers. This was confirmed by dynamic light scattering (DLS) measurements on CL_{PTXL} NPs at 30 mol% DOTAP but containing only 1 mol% PTXL: the average diameter of NPs for the sonicated sample was 180±20 nm, whereas the NPs in the unsonicated sample had an average diameter of 810±70 nm. Only a few liposomes at the upper limit of the size distribution of sonicated CL_{PTXL} NPs can be resolved by DIC microscopy (Figure 2e).

Kinetic Phase Behavior of PTXL-Loaded Cationic Liposomes

The time-dependent phase diagrams of unsonicated and sonicated PTXL-loaded CLs (DOTAP:DOPC:PTXL, 30:70-x:x mole ratio), as mapped out by DIC microscopy, are shown in Figure 3a and 3b, respectively. Blue color indicates that PTXL remained solubilized in membranes, i.e., no crystals were observed. Pink color indicates the time point at which PTXL crystals were observed. (Time points after the first observation of crystals were marked with pink color even if no further samples were assessed, since crystallization from the membrane is irreversible.) For example, in the unsonicated sample containing 5 mol% PTXL (DOTAP:DOPC:PTXL 30:65:5 mole ratio), crystals were first observed at the 4 h time point, meaning that PTXL crystallized between 2 and 4 h after hydration (Figure 3a).

The phase diagrams show that PTXL is relatively unstable within membranes when it is incorporated at > 3 mol% in DOTAP/DOPC liposomes, phase separating on a time scale of hours to one day. In contrast, samples incorporating PTXL at < 3 mol% PTXL are stable for at least a week, with unsonicated samples not phase separating within the timeline of observation (with selected samples monitored over 30 days). At 3 mol% PTXL content, PTXL-loaded CLs display moderate stability, which is reduced if the sample was subjected to sonication. Indeed, as evident from a comparison of Figure 3a (unsonicated) to Figure 3b (sonicated), sonication reduced the stability of CL_{PTXL} particles over the entire range of

PTXL contents investigated. (The black line in Figure 3b marks the boundary denoting onset of crystal formation in unsonicated samples.)

The sonicated, smaller CL_{PTXL} NPs have a much higher curvature ($C \approx 1/200\ nm^{-1}$ versus $\approx 1/800\ nm^{-1}$ for unsonicated PTXL-loaded CLs), which appears to promote faster nucleation and growth rates. A possible rationale for this observation is that high membrane curvature breaks the symmetry between the inner and outer lipid monolayers (i.e., $C_{monolayer}^{outer} > 0$ while $C_{monolayer}^{inner} < 0$ for small NPs, whereas larger, nearly flat unsonicated membranes ($C \approx 0$) have very small differences in curvature between the monolayers). This would lead to preferred PTXL partitioning into one monolayer in small NPs and thus a higher local PTXL concentration and faster nucleation time.

Synchrotron Small Angle X-Ray Scattering (SAXS)

We used SAXS to quantitatively confirm the existence of phase-separated PTXL crystals (observed in DIC) by their signature diffraction peaks [53–55]. We studied selected CL_{PTXL} NPs and DOTAP/DOPC/PTXL multilayers condensed with DNA by SAXS at different times after liposome hydration for comparison with the kinetic phase diagram results obtained by DIC and to gather detailed structural information about PTXL-containing membranes.

The top profile in Figure 4a depicts SAXS from a control sample of CLs (DOTAP:glycerol monooleate (GMO), 50:50 mole ratio) without PTXL, where only weak form factor scattering from the lipid membranes is observed. The bottom profile shows SAXS from CL_{PTXL} NPs (DOTAP:GMO:PTXL, 50:44:6 mole ratio) where three strong diffraction peaks arise from the presence of phase-separated PTXL crystals. These crystals are also optically visible in the x-ray capillary. The three characteristic PTXL diffraction peaks are located at $q_{P1} = 0.291\ Å^{-1}$, $q_{P2} = 0.373\ Å^{-1}$, and $q_{P3} = 0.436\ Å^{-1}$ in the low-q range ($0.005\ Å^{-1} < q < 0.5\ Å^{-1}$) probed in our SAXS experiment.

Independent of the lipid composition, the x-ray scattering from liposome solutions (which do not pellet from centrifugation due to the similar densities of liposome and water) is weak (Figure 4a). To overcome this problem and enable detailed structural analysis of PTXL-loaded membranes we concentrated CL_{PTXL} NPs by complexing them with oppositely charged macromolecules, using anionic DNA as the condensing agent (compare the lack of features in the range of $q = 0.05–0.25$ of Figure 4a to the well-defined peaks in same range in Figure 4c). The resulting CL_{PTXL}–DNA complexes can be further compacted into a high-membrane-concentration pellet by centrifugation. We verified that CL_{PTXL}–DNA complexes (using either plasmid DNA or short 5 base-pair double-stranded DNA) had human cancer cell death efficacy equivalent to that of CL_{PTXL} NPs (Figure 4b). We also found that a moderate change in membrane charge density (DOTAP content of 30 versus 50 mol%) had no statistically significant effect on efficacy.

In the absence of PTXL, SAXS has shown that CL–DNA complexes form the lamellar L_α^C phase for CLs composed of DOTAP and DOPC [56–59]. The multilayered structure of the L_α^C phase, consisting of onion-like NPs with diameter ≈300–400 nm, is also directly observed in cryoTEM [60,61]. Figure 4c shows SAXS profiles for CL_{PTXL}–DNA complexes

(DOTAP:DOPC:PTXL 30:70–x_{PTXL}:x_{PTXL} mole ratio; lipid/DNA charge ratio = 1.5) at x_{PTXL} = 2.75, 2.50, 2.25, and 2.00, prepared on the fourth day after liposome hydration. The observed sharp scattering peaks correspond to the (00L) peaks (L = 1,2,4, and 5) of the L_α^C phase with interlayer spacing $d_{lamellar} = 2\pi/q_{001}$ = 67 Å consisting of the combination of the thickness of the lipid bilayer (containing DOTAP, DOPC, and PTXL) and the water layer (containing a layer of DNA) [56–59]. The (003) peak is not observed because it is close to a minimum of the x-ray form factor of the CL_{PTXL}–DNA complexes. The broader shoulder peak to the right of the (001) peak at q_{DNA} = 0.112–0.116 $Å^{-1}$ is due to DNA–DNA correlations and yields an average DNA interaxial spacing $d_{DNA} = 2\pi/q_{DNA}$ = 54.0–55.9 Å [56]. The scattering from these samples containing < 3 mol% PTXL (Figure 4c) shows no evidence of PTXL-related peaks, consistent with the kinetic phase diagram (Figure 3b).

Figure 5 shows data from time-dependent SAXS studies. For each CL_{PTXL} NP sample, aliquots were freshly complexed with DNA at each time point (to avoid potential artifacts resulting from the confinement of the membranes in the CL_{PTXL}–DNA complexes) and assessed by SAXS to check for the signature PTXL crystal diffraction peaks. For samples incorporating larger amounts of PTXL (x_{PTXL} = 3, 3.5, and 4.5), the PTXL diffraction peaks appeared on or before day 4 of the experiment. This is illustrated by Figure 5(a and b), which shows the scattering profiles at four consecutive days after liposome hydration (labeled D1 through D4). The appearance of the P1 and P3 peaks is the primary indication of PTXL crystal formation for this set of data because the positions of the P2 and (004) peaks are very close together. The PTXL peaks appear on day 4 for 3.0 mol% PTXL, day 3 for 3.5 mol%, and day 2 for 4.5 mol% PTXL. All peak positions for the samples in Figure 4c and Figure 5 are reported in the Supplementary Data (Table S1).

Figure 5c shows a representative lineshape analysis for the (001) and q_{DNA} peaks (x_{PTXL} = 4.5, day 3). To get an accurate value for the peak positions, these overlapping peaks were fit simultaneously as the sum of two Lorentzian functions (dashed line). Each Lorentzian function was written as $S(q) = A/[\kappa^2 + (q-q_0)^2)]$, with q_0, κ and A as the fit parameters. The parameters q_0 and κ correspond to the peak position and the half-width at half-maximum, respectively, while A/κ^2 is the peak intensity. The background scattering (orange line) was approximated by a sloped line with the form $I^{bg}(q) = m^*q + y_0$.

Figure 5d shows a representative example fit for the (005) peak (for x_{PTXL} = 4.5, day 4), which was used to determine the lamellar interlayer spacing $d_{lamellar} = 2\pi/(q_{005}/5)$. The (005) peak was used to measure $d_{lamellar}$ because it is the highest order diffraction peak in the q-range of our SAXS study. It is expected to show the largest variation in peak position, thus yielding the most accurate measurement of changes in $d_{lamellar}$. The (005) peak was fit to a single Lorentzian with a constant background. As evident in Figures 5c and 5d, the Lorentzian fits show good agreement with the experimental scattering data, enabling an accurate measurement of peak positions.

Figure 5e shows enlarged sections of the scattering data for the sample containing 4.5 mol% PTXL in the vicinity of the (004) peak on days 1 through 4. The arrowheads in Figure 5e point to the position of q_{004} as deduced from the position of q_{005} (which has no nearby peak). On days 1 and 2, when PTXL is still soluble in the membrane, q_{004} = 0.378 $Å^{-1}$, but

on days 3 and 4, when PTXL has largely phase-separated into crystals (i.e., when the P1 and P3 diffraction peaks are strong), q_{004} = 0.375 Å^{-1}. This indicates a change in membrane thickness upon PTXL crystallization (see below). The onset of P2 at a slightly lower q (0.373 Å^{-1}, indicated by the dashed line) than q_{004} gives rise to a closely spaced doublet peak, which is quite evident from the asymmetric shape of the peak at day 3. The P2 and P3 peaks emerge on day 2 (see the small bump at the dashed line marking P2 in Figure 5e and the small P3 peak in Figure 5b (4.5% PTXL) on D2), but based on their small size and the unchanged position of q_{004} (from day 1), most of the PTXL remains soluble in the membrane.

Figure 6a displays plots of the interlayer spacing, d_{lamellar}, calculated from the 5$^{\text{th}}$ harmonic ($d_{\text{lamellar}} = 2\pi/(q_{005}/5)$), as a function of time (day 1 through day 4) for the samples with x_{PTXL} = 3, 3.5, and 4.5 mol% (DOTAP/DOPC/PTXL, 30:70–x_{PTXL}:x_{PTXL} mole ratio). The data shows an increase in d_{lamellar} from days 1 and 2 (when all PTXL is still soluble in the membranes) to days 3 and 4 (when insoluble PTXL crystals are present). An increase in d_{lamellar} implies an increase in the average membrane thickness because the thickness of the water layer containing the monolayer of DNA, electrostatically adhered to neighboring cationic membranes, is nearly constant at around 2.5 nm [56]. This increase in membrane thickness on days 3 and 4 (with PTXL crystals present) is consistent with depletion of PTXL from the membranes (i.e., replacing a DOPC molecule with a shorter PTXL molecule (see Figure 1b) is expected to thin the membrane; conversely, membranes thicken as the molar ratio of PTXL to DOPC and DOTAP decreases).

We also observed that the DNA interaxial spacing (d_{DNA}) decreases with time as PTXL crystals form on days 3 and 4 and PTXL is depleted from the membrane (Figure 6b). This decrease in d_{DNA} arises because the charge density of DOTAP/DOPC/PTXL membranes increases upon the loss of neutral PTXL from the membrane (i.e., the number of charged molecules in the membrane (DOTAP) remains constant, but the area of the membrane is reduced by the loss of PTXL). An increase in cationic membrane charge density is known to drive a decrease in d_{DNA} because the decrease in d_{DNA} increases the anionic charge density (as required to maintain overall local charge neutrality between cationic membranes and anionic DNA) [56,57,59].

Figure 6c depicts the interlayer spacing as a function of increasing PTXL content for the samples where PTXL did not phase separate (see Figure 4c), i.e., for x_{PTXL} = 2, 2.25, 2.5, and 2.75 (DOTAP/DOPC/PTXL, 30:70–x_{PTXL}:x_{PTXL} mole ratio). The data shows the expected decrease in d_{lamellar} (and thus the membrane thickness) as increasing amounts of DOPC are replaced by the shorter PTXL molecule (consistent with the behavior found in Figure 6a). Figure 6d shows that the DNA interaxial spacing increases when the PTXL content in the membrane is increased, similar to the behavior seen in Figure 6b. In this case, the number of molecules in the membrane is constant (DOPC is replaced with PTXL to increase the PTXL content). However, replacing a DOPC molecule with a shorter *but thicker* PTXL molecule (see Figure 1b) leads to an increase in the average distance between lipids (increase in the lateral area per lipid) and a lower membrane charge density. This lowering of the membrane charge density with increasing PTXL content drives the increase in DNA spacing (i.e., lowering of the anionic charge density) as noted above.

This data shows that our new methodology, of using cationic membranes complexed with oppositely charged DNA to produce highly condensed aggregates suitable for *in situ* high-resolution synchrotron SAXS studies, has enabled us to accurately detect and measure small variations in the membrane interlayer spacing and the DNA interaxial spacing due to changes in the relatively small amount of PTXL (< 5 mol%) incorporated in the cationic membranes as a function of time. After probing the time scale of PTXL solubility in membranes using optical microscopy and SAXS, we set out to correlate the observed differences between formulations incorporating varied amounts of PTXL to their drug delivery efficacy as measured by their toxicity to human cancer cell lines *in vitro*.

CL_{PTXL} NP Efficacy by Cell Viability Characterization

To begin our investigations of the efficacy of CL-based PTXL carriers (i.e. their ability to induce cancer cell death), we measured the approximate IC-50 (the drug concentration achieving half the maximal effect) for cytotoxicity in two human cancer cell lines. We obtained a baseline IC-50 value using CLs prepared from DOTAP:DOPC:PTXL at a molar ratio of 50:47:3 (to mimic the proprietary EndoTAG-1 formulation) [62]. The plots of cell survival (normalized to untreated cells) as a function of increasing PTXL concentration are shown in Figure S1 in the Supplementary Data. For PC3 cells, (prostate cancer metastasis) the IC-50 ≈ 20 nM and the cell survival curve exhibits a steep slope (between 10 and 50 nM). For the M-21 cell line (melanoma metastasis), IC-50 ≈ 45 nM with a more gradual slope (spanning the range of 5–200 nM). We found that the exact IC-50 varies with cell passage number. This is a possible source of error which we minimized by making direct numerical comparisons only between formulations that were tested side-by-side on cells of the same passage number.

In Figure S2, we show the results of an early IC-50 experiment where the PTXL concentration response was determined for both an EndoTAG-1-like liposomal formulation and for PTXL dissolved in a minimal amount of DMSO before dilution in DMEM. The results show that about four times the amount of DMSO-dissolved drug is needed to elicit the same drop in cell survival as CL_{PTXL} NPs. This effect is much larger than the observed variability in IC-50 with cell passage number.

Next, we compared the efficacy of CL-based PTXL carriers of varied composition side-by-side at the predetermined IC-50 (eliminating errors due to using cells of different passage number). For these experiments, we chose CL_{PTXL} NPs at PTXL contents covering the three different regimes of PTXL membrane solubility observed in the kinetic phase diagram (Figure 3): long-term solubility (< 3 mol% PTXL), moderate solubility (3 mol% PTXL), and low solubility (> 3 mol% PTXL). To allow a valid comparison of cell survival for NPs with different PTXL content, the total applied concentration of PTXL was fixed near the IC-50 value. Thus, CL_{PTXL} NPs with lower PTXL content in the membrane yielded correspondingly higher final molar concentrations of lipid.

Figure 7 depicts PC3 and M21 cell survival in response to 20 nM and 50 nM PTXL concentration, respectively, as a function of increasing PTXL content for CL_{PTXL} NPs with membrane composition DOTAP:DOPC:PTXL=50:50-x_{PTXL}:x_{PTXL} (molar ratio). For both cell lines, the data reveals a surprising dependence on the PTXL content. The most effective

compositions, with the lowest cell survival, are the formulations with PTXL content below 3 mol%. Cell survival is higher for particles with ≥ 3 mol% PTXL. For PC3 cells in the data shown above, cell survival decreases again above 7 mol%. This effect, where cell survival decreases for higher PTXL content formulations, has been seen for both cell lines (See the Supplementary Data Figure S3) with statistical significance, but not in every experiment (observed in three of five experiments). We attribute this to the fact that membranes which are supersaturated with PTXL exhibit significant variability as to when crystals form, because they are more sensitive to external perturbations that promote nucleation. If crystallization occurs early (within the 72 hours required for PTXL to produce its cytotoxic effect), lower efficacy would result.

The more sensitive response of PC3 cells to PTXL concentration (as illustrated by the steeper slope of the cell survival curve, see Figure S1) means that small changes in the amount of soluble/bioavailable PTXL will lead to larger differences in cell survival for PC3 than M21. This may explain the more dramatic differences in cell survival for PC3 cells treated with different liposomal formulations compared to the more incremental differences observed for M21 cells (see Figure S3).

To control for lipid toxicity—especially for CL_{PTXL} NPs at low PTXL content, where the most lipid was administered to the cells—we measured the viability of PC3 and M21 cells incubated with increasing concentrations of DOTAP/DOPC (50:50, mol:mol) small unilamellar CLs. As evident from the data shown in Figure 8, no toxicity is observed even at 100 μM total lipid, the upper limit tested in this control experiment. This is consistent with literature values for various lipids, which showed toxicity arising in the 100–200 μM range for the most toxic lipids in the study [63], while toxicity does not set in until 3000–4000 μM for the common neutral lipids mixed-chain phosphatidylcholine (egg lecithin) and dipalmitoylphosphatidylcholine (DPPC). The final total lipid concentration in our experiments probing CL_{PTXL} NP toxicity never exceeded 6 μM lipid, and therefore the observed toxicity is due to the delivered PTXL.

To verify the unexpected toxicity trends as a function of PTXL content, we expanded on the limited snapshot of information afforded by the experiments reported in Figure 7. Thus, we measured the IC-50 for cell toxicity of CL_{PTXL} NPs at PTXL contents of 1, 3, and 9 mol% for PC3 and M21 cells (Figure 9). In these experiments NPs were added to cells within 2–3 hours after hydration. For both cell lines, efficacy (diminishing of cell survival) is greatest when PTXL is incorporated at only 1 mol% (and thus more lipid is used as a carrier). The IC-50 for CL_{PTXL} NPs with 1 mol% PTXL is more than a factor of 2 lower than that for carriers with 3 mol% PTXL, both for PC3 (Figure 9a) and M21 (Figure 9b) cells. The cell survival curves for CL_{PTXL} NPs at both 1 and 9 mol% PTXL are left-shifted with respect to the baseline formulation of 3 mol% PTXL, consistent with the bell-shaped curve in Figure 7a (and Supplementary Data Figure S3). (See the caption of Figure 9 for a list of key values of p.) Thus, this data further supports the presence of two optimal activity regimes at low (≈ 1 mol%) and high (≈ 9 mol%) PTXL content.

Our kinetic phase diagram study makes it evident that the microscopic states of PTXL in membranes evolve with time spent in the aqueous milieu (i.e., from a mixed state to a

demixed state of PTXL nucleation and growth). Thus, we also investigated the efficacy of CL_{PTXL} NPs with PTXL content of 1, 3 and 9 mol% as a function of time after hydration. The data from these experiments (Figure 10) demonstrates that cells respond very differently to the same dose of PTXL depending on whether or not the PTXL is still soluble within the CL membranes. When more lipid is used to solubilize PTXL (1 mol% PTXL content), efficacy remains high (low cell survival) irrespective of time after hydration. In contrast, a significant drop in efficacy occurs (cell survival increases) over time for the CL_{PTXL} NPs at 3 and 9 mol% PTXL content.

As time progresses and the PTXL phase-separates and crystallizes (becoming biologically inert), it renders the lipid carriers with ≥ 3 mol% PTXL less and less effective, as we see in Figure 10. Based on the fact that immediately after hydration no PTXL crystals are observed, we assume that essentially all PTXL is initially associated with the CL membranes (with a small amount dissolved in water, as determined by PTXL's partition coefficient and water solubility). We thus believe that the PTXL crystals initially nucleate in the membrane but then exit (and in some cases protrude) from the membrane as the crystal grows and its size and shape can no longer be contained in the membrane. The membranes containing supersaturated PTXL will be the reservoir for PTXL crystal growth, replenishing the small amount of PTXL dissolved in the aqueous phase as it is consumed by the growth of the crystal.

The improved activity of carriers with well-solubilized PTXL (1 mol% PTXL) can be readily rationalized by the fact that the drug remains bioavailable for longer. The toxicity of PTXL requires about 72 hours to take full effect [4], and the properties of these carriers ensure that the drug will not phase separate in this period. If PTXL crystalizes from its delivery vehicle during the 72-hour window, we expect a reduction in the cytotoxicity because the concentration of bioavailable PTXL is effectively lowered. (Remember also that PTXL without a carrier is less effective (Fig. S2).) Interactions with cellular components such as membranes and cytoplasmic proteins (e.g. leading to loss of lipid from the CL carrier and thus creating a supersaturated state) may accelerate crystallization and in particular cause CL_{PTXL} NPs at the PTXL membrane solubility limit to be less stable than they appear outside of cells, e.g. in the kinetic phase diagram experiment.

Another aspect to consider for a mechanistic explanation of our findings is that the amount of lipid used to deliver a given amount of PTXL increases as the mol% PTXL in a formulation decreases. Since the particle size is constant, this results in an increased number of particles. For example, a formulation at 0.5 mol% PTXL content will contain six times as much lipid, and thus six times as many particles, as a formulation containing 3 mol% PTXL. At the same time, each of these particles will contain six times less PTXL. Since PTXL has to reach the cytoplasm to display its cytotoxic activity, our efficacy data shows that increasing the number of particles in solution increases the amount of PTXL delivered to the cytoplasm either directly from the plasma membrane or via endocytic pathways. Future cell microscopy studies will be essential to further elucidate the relevant mechanisms. It is also interesting to speculate that the known interactions of microtubules with CLs could play a role in the transfer of PTXL to the tubulin within the cell [64].

The increased efficacy that reemerges in some experiments at higher PTXL loading (~9 mol %) on short delivery time scales is highly unexpected. It may be that at this concentration, with PTXL supersaturated in the membrane, PTXL molecules are readily expelled from the lipid membranes soon after hydration. This PTXL may diffuse directly into the cell membranes, which appear as a “lipid sink.” As noted, the increased efficacy at high PTXL content was not observed in all experiments. We attribute this to the fact that membranes which are super-saturated with PTXL exhibit significant variability as to when crystals form, because they are highly sensitive to external perturbations that promote nucleation. Thus PTXL may have crystallized sooner in the experiments where efficacy of particles at 9 mol% PTXL was similar to that of particles containing 3 mol% PTXL.

Conclusions

DIC optical microscopy and high-resolution synchrotron SAXS have allowed us to map the kinetic phase behavior of DOTAP/DOPC-based CL carriers of PTXL and correlate distinct stability and efficacy regimes. To date, all efficacy studies of liposome-based PTXL carriers (including in animal models and cancer chemotherapy clinical trials) have incorporated PTXL in lipid NPs near the membrane solubility limit at 3 mol% [35,36,41,62]. In strong contrast, the work reported here shows that CL_{PTXL} NPs incorporating PTXL *below* 3 mol% have notably higher efficacy in prostate (PC3) and melanoma (M21) human cancer cells for NP delivery both on short and longer time scales (hours and days after liposome preparation). We also observed a secondary high efficacy regime on short delivery time scales for CL_{PTXL} NPs with ≥ 9 mol% PTXL in some experiments. A further significant finding of our study is that the efficacy of CL_{PTXL} NPs with higher PTXL content (≥ 3 mol %) is strongly dependent on the time between NP preparation and delivery. Our results underscore the importance of the integrated approach we present in the paper (connecting physical characterization of the particles to *in vitro* efficacy) and reveal that achieving long-term PTXL solubility (rather than maximum PTXL loading at ~3 mol%) is a key parameter in improving the efficacy of liposomal drug delivery *in vitro*.

Our experiments suggest that DOTAP/DOPC liposomes loaded with 3 mol% PTXL are still likely to phase separate on a time scale of days. This was observed in plain water, and is likely to be accelerated by perturbations in a biological environment (e.g. due to interactions with cellular components such as membranes and cytoplasmic proteins). To our knowledge, it has not yet been explored if liposomes encapsulating PTXL below its solubility limit can improve pharmacokinetics, pharmacodynamics, or biodistribution *in vivo*. Future studies will investigate how the findings we present here translate to *in vivo* efficacy and confirm them for other cell lines. It may be counterintuitive to use particles below their nominal drug-loading capacity, but our data suggests that this may facilitate actual drug targeting and enhance therapeutic outcomes for hydrophobic drugs by improving drug retention, as long as the threshold of lipid toxicity is not exceeded. As past examples demonstrate [20,21], changing the physicochemical properties of the drug delivery vehicle may significantly alter the activity of PTXL and improve its efficacy against cancers that are not currently amenable to treatment with PTXL in the Taxol or Abraxane formulations.

Finally, we presented a new methodology involving *in situ* synchrotron SAXS of PTXL-loaded cationic multilamellar membranes condensed by DNA, which has allowed us to directly confirm the presence of PTXL in membranes and to observe the incorporation and time-dependent depletion of PTXL from membranes upon PTXL crystal formation by measuring small variations in the membrane interlayer and DNA interaxial spacings. We expect this nondestructive approach to be generally applicable to other hydrophobic molecules. Besides allowing for precise measurements of the dimension of PTXL-containing membranes under realistic, bulk-water conditions, complexes of such membranes with DNA (or siRNA) constitute a promising class of dual-cargo delivery vehicles which may be used to deliver nucleic acids to work synergistically with the delivered PTXL [33].

Supplementary Material

Refer to Web version on PubMed Central for supplementary material.

Acknowledgments

This work was supported by the National Institute of Health under award GM-59288. The work was also supported in part by the National Science Foundation under award DMR-1401784 (phase behavior of cationic membranes containing PTXL). VS was supported by the National Science Foundation Graduate Research Fellowship Program under Grant No. DGE 1144085.

References

1. Wani MC, Taylor HL, Wall ME, Coggon P, McPhail AT. Plant antitumor agents. VI. Isolation and structure of taxol, a novel antileukemic and antitumor agent from Taxus brevifolia. J Am Chem Soc. 1971; 93:2325–2327. DOI: 10.1021/ja00738a045 [PubMed: 5553076]
2. Surapaneni MS, Das SK, Das NG. Designing Paclitaxel Drug Delivery Systems Aimed at Improved Patient Outcomes: Current Status and Challenges. ISRN Pharmacol. 2012; 2012:1–15. DOI: 10.5402/2012/623139
3. Schiff PB, Fant J, Horwitz SB. Promotion of microtubule assembly in vitro by taxol. Nature. 1979; 277:665–667. DOI: 10.1038/277665a0 [PubMed: 423966]
4. Jordan MA, Wendell K, Gardiner S, Brent Derry W, Copp H, Wilson L. Mitotic Block Induced in HeLa Cells by Low Concentrations of Paclitaxel (Taxol) Results in Abnormal Mitotic Exit and Apoptotic Cell Death. Cancer Res. 1996; 56:816–825. http://cancerres.aacrjournals.org/content/56/4/816.long. [PubMed: 8631019]
5. Jordan MA, Wilson L. Microtubules as a target for anticancer drugs. Nat Rev Cancer. 2004; 4:253–265. DOI: 10.1038/nrc1317 [PubMed: 15057285]
6. Jordan MA, Toso RJ, Thrower D, Wilson L. Mechanism of mitotic block and inhibition of cell proliferation by taxol at low concentrations. Proc Natl Acad Sci U S A. 1993; 90:9552–9556. http://www.ncbi.nlm.nih.gov/pubmed/8105478. [PubMed: 8105478]
7. Yvon AM, Wadsworth P, Jordan MA. Taxol suppresses dynamics of individual microtubules in living human tumor cells. Mol Biol Cell. 1999; 10:947–59. http://www.ncbi.nlm.nih.gov/pubmed/10198049. [PubMed: 10198049]
8. Markman M, Mekhail TM. Paclitaxel in cancer therapy. Expert Opin Pharmacother. 2002; 3:755–766. DOI: 10.1517/14656566.3.6.755 [PubMed: 12036415]
9. World Health Organization. 19th WHO Model List of Essential Medicines. 2015.
10. Ramalingam S, Belani CP. Paclitaxel for non-small cell lung cancer. Expert Opin Pharmacother. 2004; 5:1771–1780. DOI: 10.1517/14656566.5.8.1771 [PubMed: 15264992]
11. Hironaka S, Zenda S, Boku N, Fukutomi A, Yoshino T, Onozawa Y. Weekly paclitaxel as second-line chemotherapy for advanced or recurrent gastric cancer. Gastric Cancer. 2006; 9:14–8. DOI: 10.1007/s10120-005-0351-6 [PubMed: 16557431]

12. Sakamoto J, Matsui T, Kodera Y. Paclitaxel chemotherapy for the treatment of gastric cancer. Gastric Cancer. 2009; 12:69–78. DOI: 10.1007/s10120-009-0505-z [PubMed: 19562460]
13. Moxley KM, McMeekin DS. Endometrial carcinoma: a review of chemotherapy, drug resistance, and the search for new agents. Oncologist. 2010; 15:1026–33. DOI: 10.1634/theoncologist.2010-0087 [PubMed: 20930101]
14. Dorr RT. Pharmacology and toxicology of Cremophor EL diluent. Ann Pharmacother. 1994; 28:S11–S14. http://www.ncbi.nlm.nih.gov/pubmed/7915152. [PubMed: 7915152]
15. Weiss RB, Donehower RC, Wiernik PH, Ohnuma T, Gralla RJ, Trump DL, Baker JR, Van Echo DA, Von Hoff DD, Leyland-Jones B. Hypersensitivity reactions from taxol. J Clin Oncol. 1990; 8:1263–8. DOI: 10.1200/jco.1990.8.7.1263 [PubMed: 1972736]
16. Gelderblom H, Verweij J, Nooter K, Sparreboom A. Cremophor EL: the drawbacks and advantages of vehicle selection for drug formulation. Eur J Cancer. 2001; 37:1590–1598. DOI: 10.1016/S0959-8049(01)00171-X [PubMed: 11527683]
17. Dranitsaris G, Yu B, Wang L, Sun W, Zhou Y, King J, Kaura S, Zhang A, Yuan P. Abraxane(R) versus Taxol(R) for patients with advanced breast cancer: A prospective time and motion analysis from a Chinese health care perspective. J Oncol Pharm Pract. 2016; 22:205–211. DOI: 10.1177/1078155214556008 [PubMed: 25316611]
18. Gradishar WJ. Phase III Trial of Nanoparticle Albumin-Bound Paclitaxel Compared With Polyethylated Castor Oil-Based Paclitaxel in Women With Breast Cancer. J Clin Oncol. 2005; 23:7794–7803. DOI: 10.1200/JCO.2005.04.937 [PubMed: 16172456]
19. Rugo HS, Barry WT, Moreno-Aspitia A, Lyss AP, Cirrincione C, Leung E, Mayer EL, Naughton M, Toppmeyer D, Carey LA, Perez EA, Hudis C, Winer EP. Randomized Phase III Trial of Paclitaxel Once Per Week Compared With Nanoparticle Albumin-Bound Nab-Paclitaxel Once Per Week or Ixabepilone With Bevacizumab As First-Line Chemotherapy for Locally Recurrent or Metastatic Breast Cancer: CALGB 40502/NCCTG N0. J Clin Oncol. 2015; 33:2361–2369. DOI: 10.1200/JCO.2014.59.5298 [PubMed: 26056183]
20. Krown SE, Northfelt DW, Osoba D, Stewart JS. Use of liposomal anthracyclines in Kaposi's sarcoma. Semin Oncol. 2004; 31:36–52. DOI: 10.1053/j.seminoncol.2004.08.003
21. Hersh EM, Del Vecchio M, Brown MP, Kefford R, Loquai C, Testori A, Bhatia S, Gutzmer R, Conry R, Haydon A, Robert C, Ernst S, Homsi J, Grob JJ, Kendra K, Agarwala SS, Li M, Clawson A, Brachmann C, Karnoub M, Elias I, Renschler MF, Hauschild A. A randomized, controlled phase III trial of *nab* -Paclitaxel versus dacarbazine in chemotherapy-naïve patients with metastatic melanoma. Ann Oncol. 2015; 26:2267–2274. DOI: 10.1093/annonc/mdv324 [PubMed: 26410620]
22. Safinya CR, Ewert KK, Majzoub RN, Lia Leal C. Cationic liposome–nucleic acid complexes for gene delivery and gene silencing. New J Chem. 2014; 5164:5164–5172. DOI: 10.1039/c4nj01314j
23. Allen TM, Cullis PR. Liposomal drug delivery systems: From concept to clinical applications. Adv Drug Deliv Rev. 2013; 65:36–48. DOI: 10.1016/j.addr.2012.09.037 [PubMed: 23036225]
24. Sercombe L, Veerati T, Moheimani F, Wu SY, Sood AK, Hua S. Advances and Challenges of Liposome Assisted Drug Delivery. Front Pharmacol. 2015; 6:286.doi: 10.3389/fphar.2015.00286 [PubMed: 26648870]
25. Charrois GJ, Allen TM. Drug release rate influences the pharmacokinetics, biodistribution, therapeutic activity, and toxicity of pegylated liposomal doxorubicin formulations in murine breast cancer. Biochim Biophys Acta - Biomembr. 2004; 1663:167–177. DOI: 10.1016/j.bbamem.2004.03.006
26. Drummond DC, Meyer O, Hong K, Kirpotin DB. Optimizing Liposomes for Delivery of Chemotherapeutic Agents to Solid Tumors. Pharmacol Rev. 1999; 51:692–743. http://www.pharmrev.org.
27. Fritze A, Hens F, Kimpf A, Schubert R, Peschka-Süss R. Remote loading of doxorubicin into liposomes driven by a transmembrane phosphate gradient. Biochim Biophys Acta. 2006; 1758:1633–1640. DOI: 10.1016/j.bbamem.2006.05.028 [PubMed: 16887094]
28. Koudelka Š, Turánek J. Liposomal paclitaxel formulations. J Control Release. 2012; 163:322–334. DOI: 10.1016/j.jconrel.2012.09.006 [PubMed: 22989535]

29. Campbell RB, Balasubramanian SV, Straubinger RM. Influence of cationic lipids on the stability and membrane properties of paclitaxel-containing liposomes. J Pharm Sci. 2001; 90:1091–1105. DOI: 10.1002/jps.1063 [PubMed: 11536214]
30. Hong S-S, Choi JY, Lee M-K, Kim SH, Lim S-J. Development of paclitaxel-loaded liposomal nanocarrier stabilized by triglyceride incorporation. Int J Nanomedicine. 2016; 1:4465–4477. DOI: 10.2147/IJN.S113723
31. Kannan V, Balabathula P, Divi MK, Thoma LA, Wood GC. Optimization of drug loading to improve physical stability of paclitaxel-loaded long-circulating liposomes. J Liposome Res. 2015; 25:308–315. DOI: 10.3109/08982104.2014.995671 [PubMed: 25541107]
32. Bernsdorff C, Reszka R, Winter R. Interaction of the anticancer agent Taxol (paclitaxel) with phospholipid bilayers. J Biomed Mater Res. 1999; 46:141–149. DOI: 10.1002/(SICI)1097-4636(199908)46:2<141::AID-JBM2>3.0.CO;2-U [PubMed: 10379991]
33. Steffes VM, Ewert KK, Safinya CR. No Title, Unpubl Data. n.d
34. Ait-Oudhia S, Mager DE, Straubinger RM. Application of pharmacokinetic and pharmacodynamic analysis to the development of liposomal formulations for oncology. Pharmaceutics. 2014; 6:137–174. DOI: 10.3390/pharmaceutics6010137 [PubMed: 24647104]
35. Fetterly GJ, Straubinger RM. Pharmacokinetics of paclitaxel-containing liposomes in rats. Am Assoc Pharm Sci Pharm Sci Technol. 2003; 5:90–100. DOI: 10.1208/ps050432
36. Sharma A, Sharma US, Straubinger RM. Paclitaxel-liposomes for intracavitary therapy of intraperitoneal P388 leukemia. Cancer Lett. 1996; 107:265–272. [PubMed: 8947523]
37. Sharma A, Mayhew E, Straubinger RM. Antitumor Effect of Taxol-containing Liposomes in a Taxol-resistant Murine Tumor Model Advances in Brief Liposomes in a Taxol-resistant Murine Tumor. Cancer Res. 1993; 53:5877–5881. [PubMed: 7903197]
38. Zhou R, Mazurchuk RV, Tamburlin JH, Harrold JM, Mager DE, Straubinger RM. Differential pharmacodynamic effects of paclitaxel formulations in an intracranial rat brain tumor model. J Pharmacol Exp Ther. 2010; 332:479–88. DOI: 10.1124/jpet.109.160044 [PubMed: 19861574]
39. Xu X, Wang L, Xu H-Q, Huang X-E, Qian Y-D, Xiang J. Clinical comparison between paclitaxel liposome (Lipusu®) and paclitaxel for treatment of patients with metastatic gastric cancer. Asian Pacific J Cancer Prev. 2013; 14:2591–4. http://www.ncbi.nlm.nih.gov/pubmed/23725180.
40. Wang H, Cheng G, Du Y, Ye L, Chen W, Zhang L, Wang T, Tian J, Fu F. Hypersensitivity reaction studies of a polyethoxylated castor oil-free, liposome-based alternative paclitaxel formulation. Mol Med Rep. 2013; 7:947–952. DOI: 10.3892/mmr.2013.1264 [PubMed: 23291923]
41. Zhang JA, Anyarambhatla G, Ma L, Ugwu S, Xuan T, Sardone T, Ahmad I. Development and characterization of a novel Cremophor® EL free liposome-based paclitaxel (LEP-ETU) formulation. Eur J Pharm Biopharm. 2005; 59:177–187. DOI: 10.1016/j.ejpb.2004.06.009 [PubMed: 15567316]
42. Schmitt-Sody M, Strieth S, Krasnici S, Sauer B, Schulze B, Teifel M, Michaelis U, Naujoks K, Dellian M. Neovascular Targeting Therapy: Paclitaxel Encapsulated in Cationic Liposomes Improves Antitumoral Efficacy. Clin Cancer Res. 2003; 9:2335–2341. [PubMed: 12796403]
43. Crosasso P, Ceruti M, Brusa P, Arpicco S, Dosio F, Cattel L. Preparation characterization and properties of sterically stabilized paclitaxel-containing liposomes. J Control Release. 2000; 63:19–30. DOI: 10.1016/S0168-3659(99)00166-2 [PubMed: 10640577]
44. Kan P, Tsao C-W, Wang A-J, Su W-C, Liang H-F. A liposomal formulation able to incorporate a high content of Paclitaxel and exert promising anticancer effect. J Drug Deliv. 2011; 2011:629234.doi: 10.1155/2011/629234 [PubMed: 21490755]
45. Koudelka Š, Turánek-Knötigová P, MaŠek J, Korvasová Z, Škrabalová M, Plocková J, Bartheldyová E, Turánek J. Liposomes With High Encapsulation Capacity for Paclitaxel: Preparation, Characterisation and In Vivo Anticancer Effect. J Pharm Sci. 2010; 99:2309–2319. DOI: 10.1002/jps.21992 [PubMed: 19904827]
46. Balasubramanian SV, Straubinger RM. Taxol-Lipid Interactions- Taxol-Dependent Effects on the Physical Properties of Model Membranes. Biochim Biophys Acta. 1994; 33:8941–8947. http://pubs.acs.org/doi/pdf/10.1021/bi00196a011?source=chemport%5Cnpapers2://publication/uuid/45662A2C-81C0-44D5-A125-3D85D379D53A.

47. Yang T, Choi M-K, Cui F-D, Lee S-J, Chung S-J, Shim C-K, Kim D-D. Antitumor Effect of Paclitaxel-Loaded PEGylated Immunoliposomes Against Human Breast Cancer Cells. Pharm Res. 2007; 24:2402–2411. DOI: 10.1007/s11095-007-9425-y [PubMed: 17828616]
48. Thurston G, Mclean JW, Rizen M, Baluk P, Haskell A, Murphy TJ, Hanahan D, Mcdonald DM. Cationic Liposomes Target Angiogenic Endothelial Cells in Tumors and Chronic Inflammation in Mice. J Clin Invest. 1998; 101:1401–1413. http://www.jci.org. [PubMed: 9525983]
49. Dellian M, Yuan F, Trubetskoy V, Torchilin V, Jain R. Vascular permeability in a human xenograft: molecular charge dependence. Br J Cancer. 2000; 82:1513–1518. https://www.ncbi.nlm.nih.gov/pmc/articles/PMC2363402/pdf/82-6691171a.pdf. [PubMed: 10789717]
50. Campbell RB, Fukumura D, Brown EB, Mazzola LM, Izumi Y, Jain RK, Torchilin VP, Munn LL. Cationic charge determines the distribution of liposomes between the vascular and extravascular compartments of tumors. Cancer Res. 2002; 62:6831–6836. http://www.ncbi.nlm.nih.gov/pubmed/12460895. [PubMed: 12460895]
51. Awada A, Bondarenko IN, Bonneterre J, Nowara E, Ferrero JM, Bakshi AV, Wilke C, Piccart M. A randomized controlled phase II trial of a novel composition of paclitaxel embedded into neutral and cationic lipids targeting tumor endothelial cells in advanced triple-negative breast cancer (TNBC). Ann Oncol. 2014; 25:824–831. DOI: 10.1093/annonc/mdu025 [PubMed: 24667715]
52. Leal C, Ewert KK, Bouxsein NF, Shirazi RS, Li Y, Safinya CR, Sima O, Golan Y, Danielsson M. Stacking of short DNA induces the gyroid cubic-to-inverted hexagonal phase transition in lipid–DNA complexes. Soft Matter. 2013; 9:795–804. DOI: 10.1039/C2SM27018H [PubMed: 23476712]
53. Mastropaolo D, Camerman A, Luo Y, Brayer GD, Camerman N. Crystal and molecular structure of paclitaxel (taxol). Proc Natl Acad Sci U S A. 1995; 92:6920–6924. http://www.ncbi.nlm.nih.gov/pubmed/7624344. [PubMed: 7624344]
54. Cavalcanti LP, Konovalov O, Haas H. X-ray diffraction from paclitaxel-loaded zwitterionic and cationic model membranes. Chem Phys Lipids. 2007; 150:58–65. DOI: 10.1016/j.chemphyslip.2007.06.219 [PubMed: 17662973]
55. Kenth S, Sylvestre J-P, Fuhrmann K, Meunier M, Leroux J-C. Fabrication of Paclitaxel Nanocrystals by Femtosecond Laser Ablation and Fragmentation. J Pharm Sci. 2011; 100:1022–1030. DOI: 10.1002/jps.22335 [PubMed: 20809524]
56. Rädler JO, Koltover I, Salditt T, Safinya CR. Structure of DNA-Cationic Liposome Complexes: DNA Intercalation in Multilamellar Membranes in Distinct Interhelical Packing Regimes. Science (80-). 1997; 275:810. http://science.sciencemag.org/content/275/5301/810.long.
57. Salditt T, Koltover I, Rädler JO, Safinya CR. Two-Dimensional Smectic Ordering of Linear DNA Chains in Self-Assembled DNA-Cationic Liposome Mixtures. Phys Rev Lett. 1997; 79:2582–2585. http://www.mrl.ucsb.edu/~safinyaweb/PDFs/publications_PDF/1997_PRL_1997_79_2582_smectic_complexes_salditt_Safinya.pdf.
58. Koltover I, Salditt T, Rädler JO, Safinya CR. An Inverted Hexagonal Phase of Cationic Liposome-DNA Complexes Related to DNA Release and Delivery. Science (80-). 1998; 281:78–81. http://science.sciencemag.org/content/281/5373/78.long.
59. Koltover I, Salditt T, Safinya CR. Phase Diagram, Stability, and Overcharging of Lamellar Cationic Lipid–DNA Self-Assembled Complexes. Biophys J. 1999; 77:915–924. http://www.mrl.ucsb.edu/~safinyaweb/PDFs/publications_PDF/1999_biophys_j_1999_77_915_safinya_cl_dna.pdf. [PubMed: 10423436]
60. Majzoub RN, Chan C-L, Ewert KK, Silva BFB, Liang KS, Jacovetty EL, Carragher B, Potter CS, Safinya CR. Uptake and transfection efficiency of PEGylated cationic liposome–DNA complexes with and without RGD-tagging. Biomaterials. 2014; 35:4996–5005. DOI: 10.1016/j.biomaterials.2014.03.007 [PubMed: 24661552]
61. Battersby BJ, Grimm R, Huebner S, Cevc G. Evidence for three-dimensional interlayer correlations in cationic lipid-DNA complexes as observed by cryo-electron microscopy. Biochim Biophys Acta - Biomembr. 1998; 1372:379–383. DOI: 10.1016/S0005-2736(98)00062-5
62. Strieth S, Nussbaum CF, Eichhorn ME, Fuhrmann M, Teifel M, Michaelis U, Berghaus A, Dellian M. Tumor-selective vessel occlusions by platelets after vascular targeting chemotherapy using paclitaxel encapsulated in cationic liposomes. Int J Cancer. 2008; 122:452–460. DOI: 10.1002/ijc.23088 [PubMed: 17918179]

63. Mayhew E, Ito M, Lazo R. Toxicity of non-drug-containing liposomes for cultured human cells. Exp Cell Res. 1987; 171:195–202. DOI: 10.1016/0014-4827(87)90262-X [PubMed: 3622630]

64. Raviv, U., Needleman, DJ., Li, Y., Miller, HP., Wilson, L., Safinya, CR., Fisher, ME. [accessed July 17, 2017] Cationic liposome–microtubule complexes: Pathways to the formation of two-state lipid–protein nanotubes with open or closed ends. n.d. http://www.mrl.ucsb.edu/~safinyaweb/PDFs/publications_PDF/2005_pnas_2005_102_11167_safinya_raviv_CL_MT_complexes.pdf

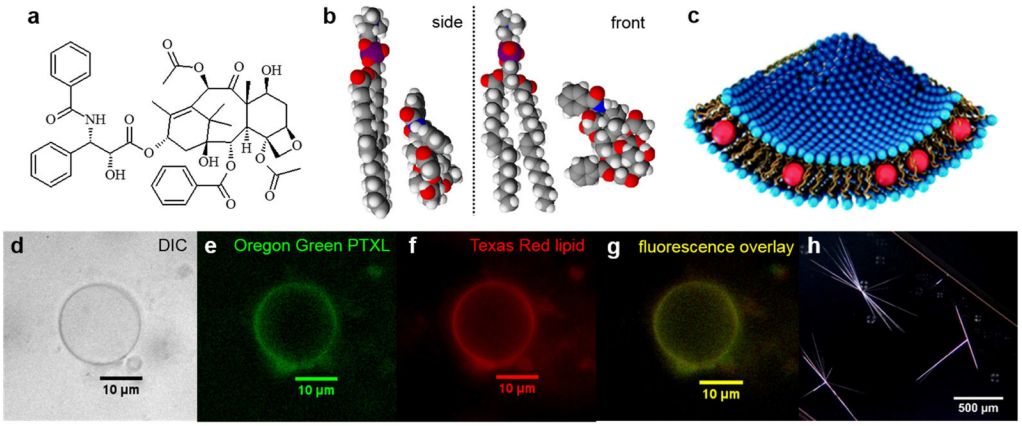

Figure 1.

PTXL-containing liposomes from the molecular to micrometer scale. (a–c) a molecular look at the PTXL–lipid system: a) the chemical structure of PTXL, b) space filling molecular models for DOPC and PTXL viewed from the side and the front, c) schematic drawing of a liposome with hydrophobic molecules (red spheres, representative of PTXL) embedded within the membrane. (d–f) Microscopy images of a singular unsonicated PTXL-containing liposome (composed of a 90:10:5:7.1 mole ratio of DOTAP:DOPC:OregonGreen-PTXL:TexasRed-DHPE), demonstrating colocalization of PTXL with the lipid bilayer: d) differential-interference-contrast image, e) green fluorescence due to Oregon Green-conjugated PTXL, f) red fluorescence from the Texas Red–DHPE lipid label, g) fluorescence overlay of Oregon Green PTXL and Texas Red lipid. (h) Polarized optical microscopy image of PTXL crystals that have phase separated from unsonicated liposomes (5:92:3 initial mole ratio of DOTAP/DOPC/PTXL) five days after hydration.

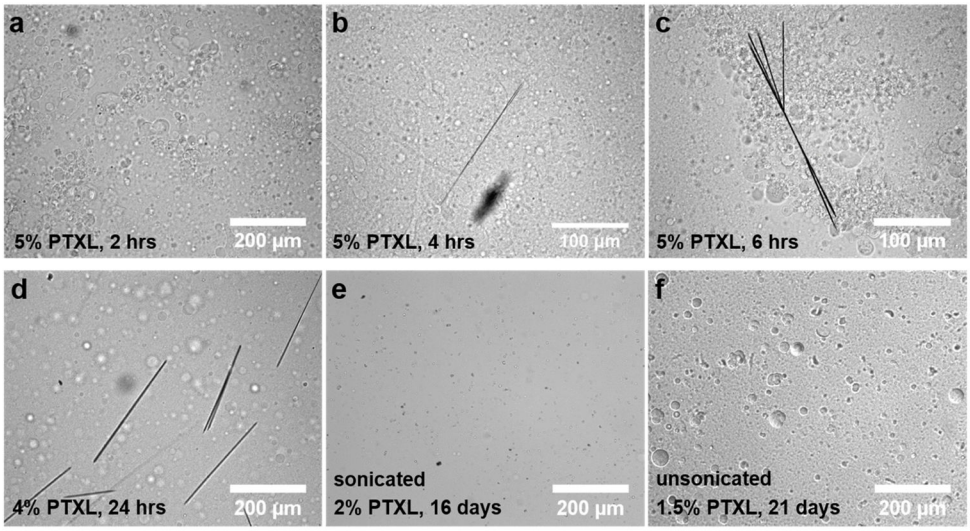

Figure 2.

DIC microscopy images of liposomes and crystallized PTXL. Unless otherwise specified, samples are unsonicated liposomes made of DOTAP, DOPC and PTXL (30:70–x_{PTXL}:x_{PTXL} mole ratio). (a–c) Images of liposomes with x_{PTXL}=5 taken a) 2 h, b) 4 h, and c) 6 h after hydration; crystal formation is evident at 4 h, indicating the short period of stability at high PTXL contents. (d) Image of a sample with x_{PTXL}=4, showing PTXL crystals at 24 h after hydration. (e and f) Images of samples that exhibit longer-term PTXL solubility: e) x_{PTXL}=2, sonicated sample with an average particle size < 200 nm, and f) x_{PTXL}=1.5, unsonicated sample composed of larger multilamellar vesicles (≈ 800 nm average diameter).

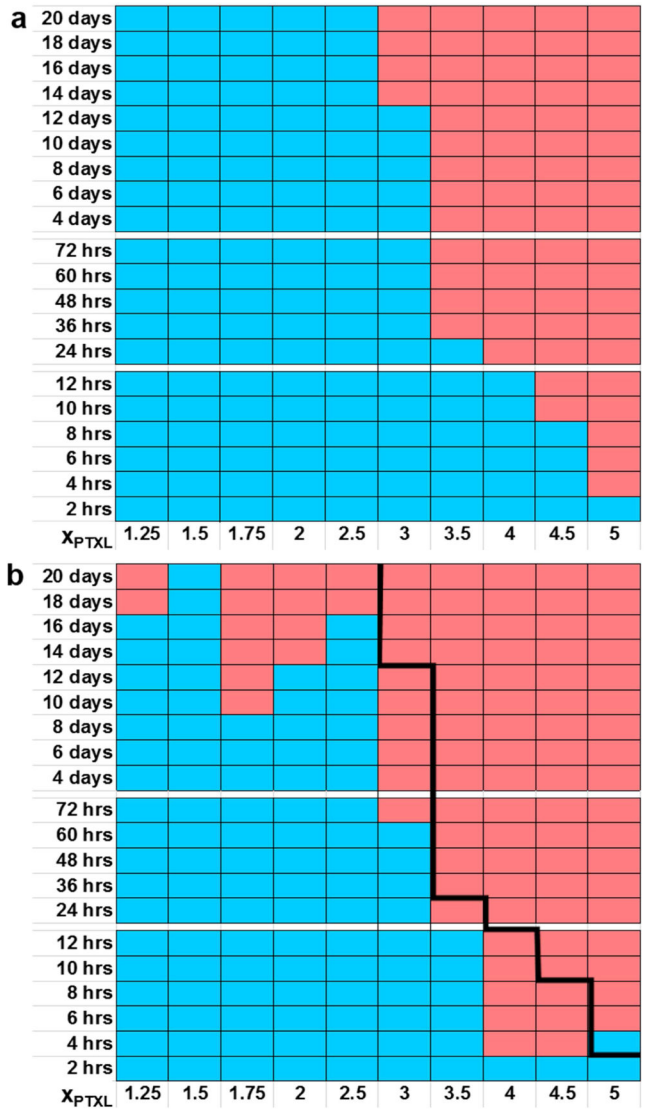

Figure 3.

Kinetic phase diagrams of PTXL solubility in CL_{PTXL} NPs prepared from DOTAP, DOPC and PTXL (30:70–x_{PTXL}:x_{PTXL} mole ratio). DIC microscopy (see Figure 2) was used to assess whether PTXL crystallization had occurred at the indicated times after hydration. Blue color indicates absence of PTXL crystals (PTXL remained soluble in the membranes), while pink color indicates presence of PTXL crystals. (a) Stability of PTXL in *unsonicated* liposomes. (b) Stability of PTXL in *sonicated* liposomes. The black line, showing the solubility boundary for unsonicated liposomes, is included as a reference to facilitate comparison.

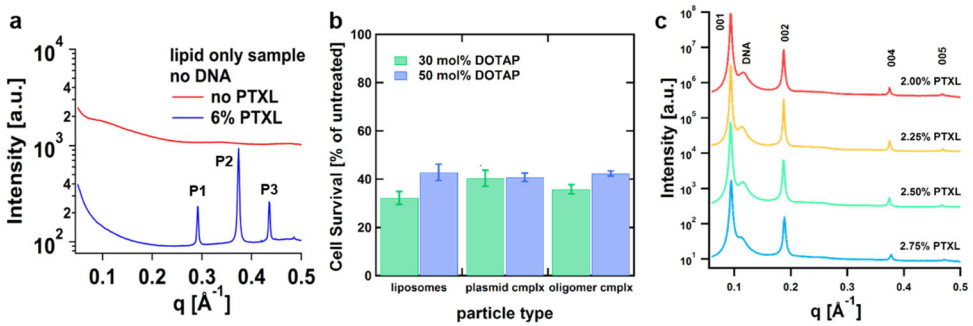

Figure 4.

X-ray scattering and cell survival studies of CL_{PTXL} NPs compared to CL_{PTXL}-DNA complexes. (a) Representative examples of the average scattering intensity for uncondensed (DNA-free) lipid samples without PTXL (red) and CL_{PTXL} NPs with high PTXL content (blue). Only the scattering form factor appears for the lipid sample when the lipid bilayers are not condensed. When PTXL has crystallized (blue curve), peaks due to PTXL crystals are observed at P1 (q=0.291 Å^{-1}), P2 (q=0.373 Å^{-1}), and P3 (q=0.436 Å^{-1}). (b) Cell survival outcomes of PC3 cells treated with 50 nM PTXL in either CL_{PTXL} liposomes or CL_{PTXL}–DNA complexes show no significant differences in efficacy due to complex formation (with either plasmid or short oligomeric DNA) or lipid charge density (30% DOTAP vs. 50% DOTAP). (c) Small angle x-ray scattering intensity for four CL_{PTXL} NP samples with high PTXL solubility (PTXL content < 3 mol%; DOTAP/DOPC/PTXL, 30:70–x_{PTXL}:x_{PTXL} mole ratio) that were condensed with DNA on the fourth day after hydration. In these samples, PTXL remains soluble (no P1, P2 or P3 peaks are observed). However, because the samples have been condensed with DNA, the (001), (002), (004), and (005) peaks characteristic of the $L_\alpha{}^C$ phase appear, along with the broad DNA–DNA correlation peak, as labeled.

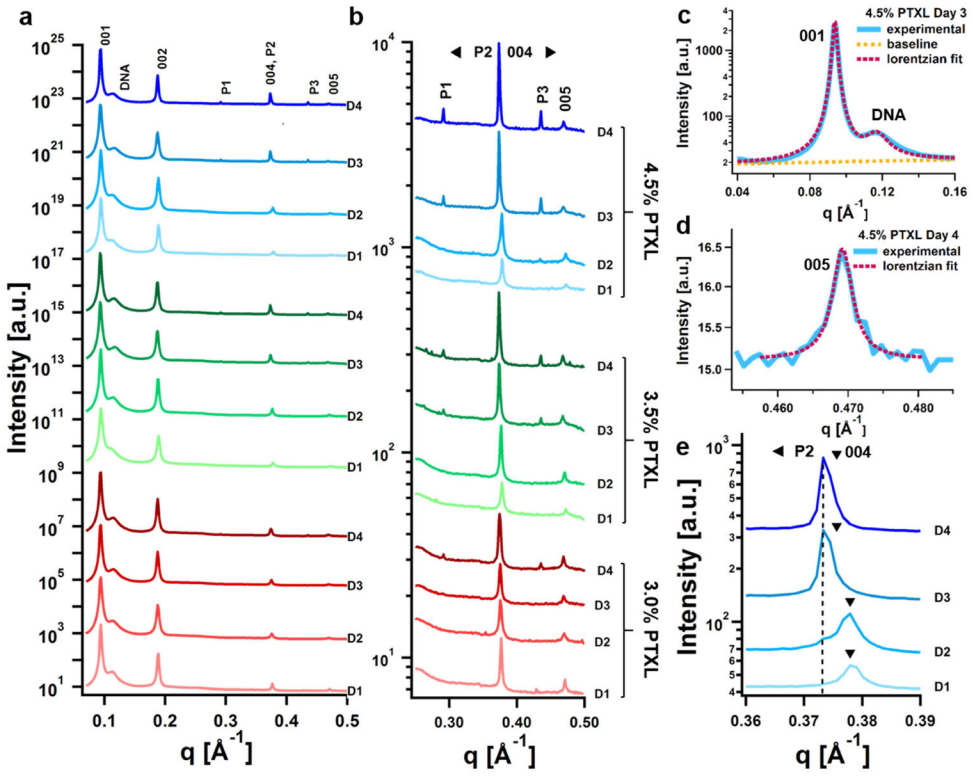

Figure 5.

X-ray scattering analysis of PTXL crystallization from CL_{PTXL} NPs. Scattering intensity is plotted for samples containing 3.0 (red lines), 3.5 (green lines), and 4.5 (blue lines) mol% PTXL (DOTAP/DOPC/PTXL, 30:70–x_{PTXL}:x_{PTXL} mole ratio). Over the course of 4 d following hydration, aliquots of the CL_{PTXL} NPs were condensed with DNA each day (day of scan designated on graphs as D1–D4) and formation of PTXL crystals was assessed with SAXS. (a) Full scattering spectra for all samples over the investigated range of the scattering vector q (q=0.05–0.5 Å^{-1}). Peaks originating from the stacked membranes of the lamellar $L_\alpha{}^C$ structure are labeled as 001, 002, 004, and 005, while the DNA–DNA correlation peak is marked DNA, and P1, P2, P3 mark peaks originating from PTXL crystals (see Figure 4). (b) Expanded view of the plots in (a) around the PTXL peaks (q=0.25–0.50 Å^{-1}). The appearances of peaks at P1 and P3 are the clearest indication of the presence of PTXL crystals. (c) An example of peak fitting for the (001) and q_{DNA} peaks. The dashed line indicates a background-subtracted fit as the sum of two Lorentzian functions. The background scattering is shown by the orange dashed line with the form $I^{bg}(q) = m^*q + y_0$. Each Lorentzian function was written as $S(q) = A/[\kappa^2 + (q-q_0)^2)]$, where q_0 and κ correspond to the peak position and the HWHM (half width at half maximum), respectively. For the (001) SAXS peak, $A_{001} = 3.80 \times 10^{-3}$, $q_{001} = 0.09374$ Å^{-1}, $\kappa_{002} = 1.16 \times 10^{-3}$ Å^{-1}; for the q_{DNA} SAXS peak, $A_{DNA} = 1.36 \times 10^{-3}$, $q_{DNA} = 0.1168$ Å^{-1}, $\kappa_{DNA} = 6.64 \times 10^{-3}$ Å^{-1}. (d) Example fit for the (005) peak, which was used to determine the interlayer lamellar distance (the sum of the membrane bilayer thickness and the DNA containing water layer). The (005) peak was fit to a single Lorentzian with a constant background scattering of y_0 = 15.1, where $A_{005} = 3.97 \times 10^{-6}$, $q_{005} = 0.4692$ Å^{-1}, and $\kappa_{005} = 1.70 \times 10^{-3}$ Å^{-1}. In this

particular series of samples (30 mol% DOTAP, DOTAP/DNA charge ratio of 1.5), the prominent P2 peak overlaps the (004) peak. (e) Expanded view of the region around the P2 and (004) peaks (4.5 mol% PTXL, days 1–4). The black arrowheads indicate the predicted position of the (004) peak for each sample, based on the position of the (005) peak. As PTXL leaves the membrane, the (004) peak shifts to lower q (corresponding to a thickening of the membrane), toward the P2 peak (position indicated by dashed line) which appears as the PTXL crystals form.

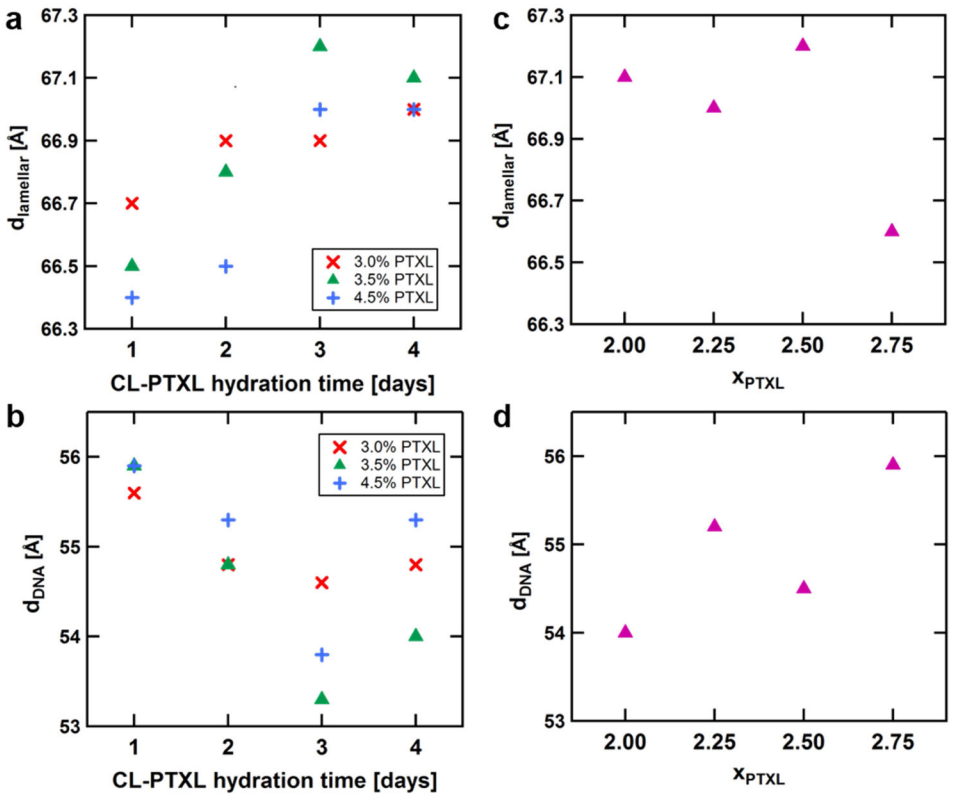

Figure 6.

Lamellar interlayer distance and DNA interaxial spacing for DOTAP/DOPC/PTXL samples (30:70–x_{PTXL}:x_{PTXL} mole ratio) condensed with DNA as derived from x-ray lineshape analysis. (a, b) Plots of $d_{lamellar}$ (a) and d_{DNA} (b) as a function of time for samples which exhibited PTXL crystallization. (c, d) Plots of $d_{lamellar}$ (c) and d_{DNA} (d) against PTXL content for the stable samples (no PTXL crystallization; < 3 mol% PTXL) on day 4. The lamellar interlayer distance $d_{lamellar}$ is the sum of the thicknesses of the lipid bilayer and the DNA-containing water layer. It was calculated from the position of the (005) peak as $d_{lamellar} = 2\pi/(q_{005}/5)$. The DNA–DNA spacing was calculated from the DNA–DNA correlation peak ($d_{DNA}=2\pi/q_{DNA}$). See text for discussion.

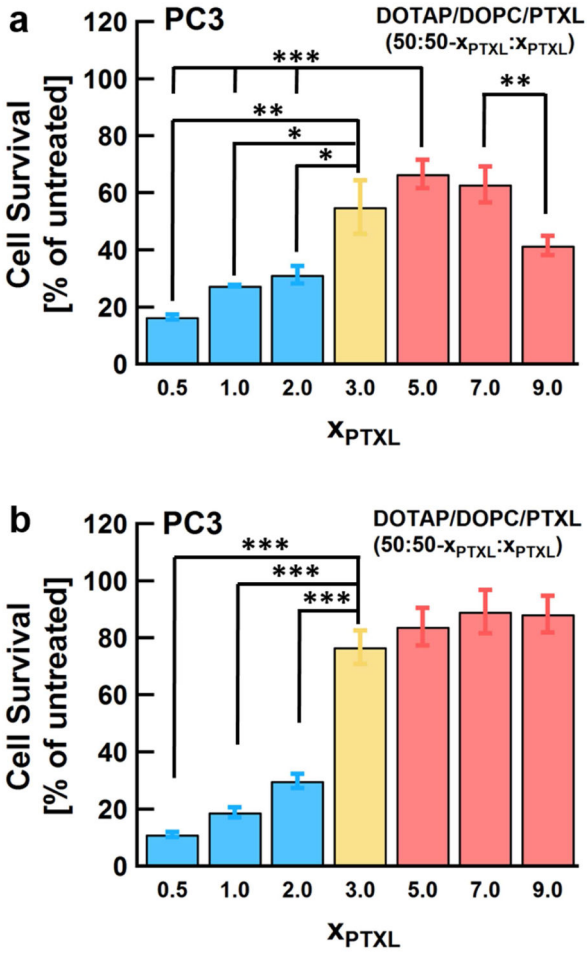

Figure 7.

Cell survival data for CL_{PTXL} NPs of varied PTXL content in two human cancer cell lines. The total concentration of PTXL applied to cells was kept constant at 20 nM for PC3 prostate cancer cells (a) and 50 nM for M21 melanoma cells (b). These concentrations are near the IC-50s for PTXL in EndoTAG-1-like NPs, which were determined in previous experiments to assess the sensitivity of each cell line to PTXL. Because the total amount of applied PTXL was constant, the amount of applied lipid decreased as the PTXL content increased. Cell viability was measured 72 h after the NPs were added to cells and is normalized to that of untreated cells. The color bars indicate the PTXL membrane solubility at each x_{PTXL} value (blue: more soluble, i.e. PTXL content < 3 mol%; yellow: moderate solubility, i.e. PTXL content = 3 mol%; pink: low PTXL solubility, i.e. PTXL content > 3 mol%). Statistical significance (Student T-test) is indicated by asterisks: (*) $0.05 < p < 0.08$, (**) $0.01 < p < 0.05$, (***) $p < 0.01$.

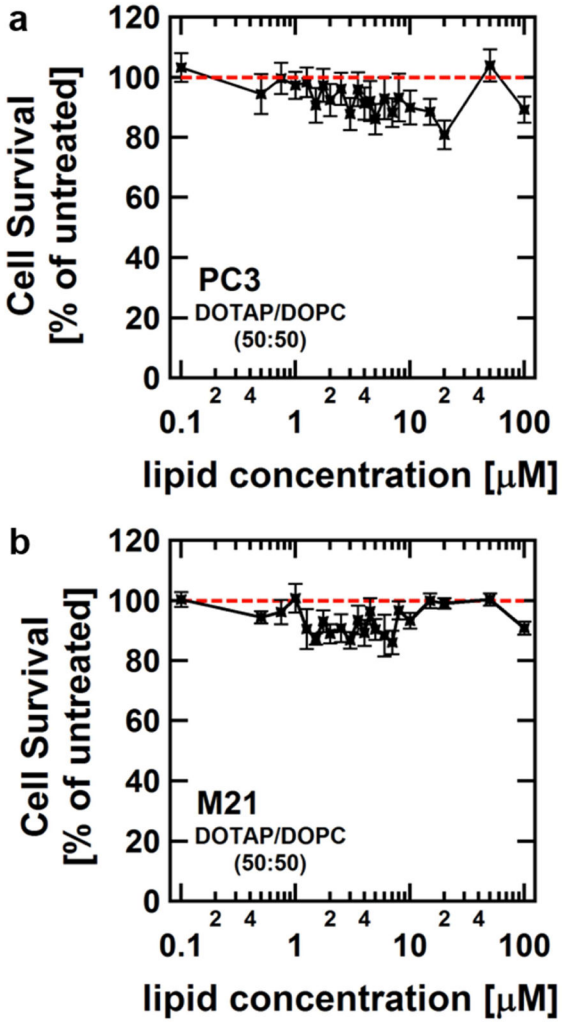

Figure 8.

Assessment of lipid toxicity in a) PC3 cells (human prostate cancer) and b) M21 cells (human melanoma). Liposomes consisting of DOTAP and DOPC (1:1 mole ratio) were diluted in DMEM from 100 to 0.1 μM total lipid and added to cells. Cell viability was measured 72 h after the liposomes were added to the cells and is normalized to that of untreated cells. No lipid toxicity is apparent in this concentration range.

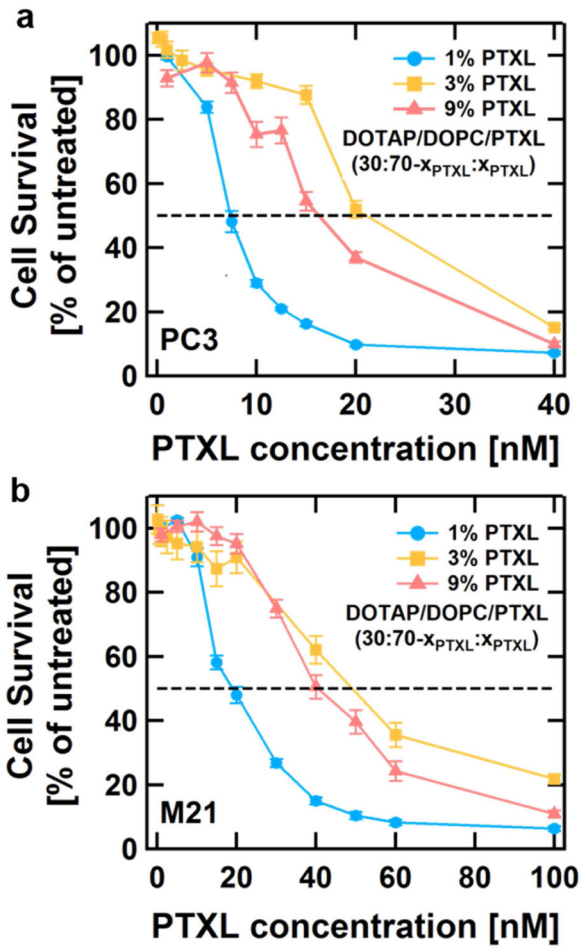

Figure 9.

Cell survival as a function of PTXL concentration for CL_{PTXL} NPs containing 1, 3 or 9 mol % PTXL added to a) PC3 cells and b) M21 cells. The dashed line indicates 50% cell death. For PC3 cells, the IC-50 is highest (about 20 nM) for 3 mol% PTXL, and lower for both 1 mol% PTXL (about 7.5 nM) and 9 mol% PTXL (about 15 nM). For PC3, the Student T-test indicates statistical significance of $p<0.01$ for pairwise comparison of all three data points at 10, 15 and 20 nM. The IC-50 in M21 cells is also highest (about 50 nM) for 3 mol% PTXL, but lower for 1 mol% PTXL (about 20 nM) and 9 mol% PTXL (about 40 nM). For M21, $p<0.01$ for 1 mol% PTXL compared to 3 or 9 mol% PTXL at 40 nM and 60 nM, and for 3 mol% PTXL compared to 9 mol% PTXL, $p=0.015$ and $p=0.026$ at 40 nM and 60 nM, respectively.

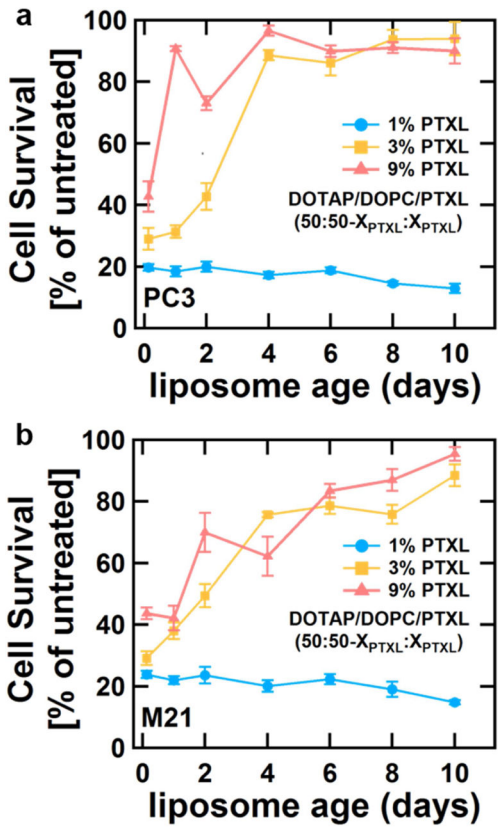

Figure 10.

Cell survival data for CL_{PTXL} NPs with selected PTXL content in two human cancer cell lines as a function of time after hydration in water. The total concentration of PTXL applied to cells was kept constant at 22.5 nM for PC3 cells (a) and 65.0 nM for M21 cells (b). The CL_{PTXL} NPs containing 1 (blue), 3 (yellow), or 9 (pink) mol% PTXL (50 mol% DOTAP) were hydrated and sonicated at different time points leading up to the experiment to be applied to the cells at the same time. Cell viability was measured 72 h after the NPs were added to cells and is normalized to that of untreated cells.